INFORMATICS JOURNALS
The Journal of Electrochemical Society of India, Volume 75, Issue (1&2), January-March 2026; pp. 57–66
ISSN (Print) : 0013-466X
ISSN (Online) : xxxx-xxxx
DOI: 10.18311/JESCI/2026/67829

Oxygen-Incorporated Defect-Rich 2H-MoS_2 Nanosheets on Nitrogen, Phosphorus-Doped rGO as an Effective Electrocatalyst for Hydrogen Evolution Reaction

K. Guruprasad and T. Maiyalagan*

Electrochemical Energy Laboratory, Department of Chemistry, SRM Institute of Science and Technology, Kattankulathur – 603203, Tamil Nadu, India

Abstract

Significant effort has been taken to improve the Hydrogen Evolution Reaction (HER) to make the hydrogen fuel economy possible. Although Pt based catalysts exhibit excellent HER activity, their high cost and limited availability hinder their large-scale application. Therefore, developing efficient, low-cost, and earth-abundant transition metal based electrocatalysts has become an important research focus. This study implements the concept of incorporating oxygen in the Molybdenum Disulfide (MoS_2) and making a nanocomposite with Nitrogen and Phosphorus-doped Reduced Graphene Oxide. The O-MoS_2/N, P-rGO synthesis strategy involves a facile hydrothermal method for MoS_2 and the preparation of heteroatom-doped graphene by high-temperature heating. The resulting composite of O-MoS_2 with N, P-rGO outperforms the other O-MoS_2-based nanocomposite and bare O-MoS_2 towards electrochemical HER activity by exhibiting an onset potential of 110 mV, an overpotential of 160 mV measured at 10 mA/cm^2 and a Tafel slope value of 87 mV/dec. The optimized O-MoS_2/N, P-rGO exhibits a high current density of 100 mA/cm^2 at the minimum overpotential of 250 mV and demonstrates near stable performance with minimal overpotential difference of 20 mV after continuous 1000 cycles.

Keywords: Heteroatom-doped Graphene, N, P-rGO, Nanocomposite, O-MoS_2

1. Introduction

Hydrogen energy is widely recognised as a promising secondary energy source. It is expected to replace conventional fossil fuels in the near future because of its clean, sustainable, and high energy density characteristics[1,2]. Among the various hydrogen production technologies, electrochemical water splitting, particularly the HER, has emerged as one of the most efficient, economical, and environmentally benign approaches due to its carbon-free emission process[3]. Platinum-based noble metals exhibit outstanding electrocatalytic activity toward HER; however, their scarcity and high cost severely restrict large-scale commercial applications[4–7]. Therefore, significant research efforts have been devoted to the development of low-cost, earth-abundant, and highly efficient non-noble-metal electrocatalysts for hydrogen generation[8–12]. Transition Metal Dichalcogenides (TMD) have attracted considerable attention as promising HER electrocatalysts[13]. In particular, transition metal-based compounds such as borides, carbides, nitrides, sulfides, and phosphides containing Fe, Ni, Co, Mo, and W have been extensively investigated for efficient hydrogen production[14–23]. Among these materials, MoS_2, possessing a layered hexagonal structure analogous to graphite, has demonstrated promising HER activity mainly originating from its edge sites rather than the inert basal planes[24–27]. However, the practical catalytic performance of MoS_2 remains far inferior to that of Pt/C catalysts because of its intrinsically poor electrical conductivity and limited number of exposed active sites[28,29].

*Email: maiyalagan@gmail.com

To overcome these limitations, several strategies have been explored to enhance the electrocatalytic performance of MoS_2, including increasing the density of exposed edge sites, defect engineering, phase transformation, transition-metal doping, and incorporation of heteroatoms or vacancies to optimize hydrogen adsorption energy[30–34]. Dai and co-workers synthesised MoS_2/reduced graphene oxide hybrids exhibiting superior HER performance owing to the enhanced exposure of catalytic edge sites[35]. Similarly, Tour's group fabricated edge-oriented MoS_2 films through sulfurization of sponge-like molybdenum oxide films on Mo substrates, resulting in improved electrocatalytic activity and long-term stability. Xie *et al.* further demonstrated that oxygen incorporation into MoS_2 effectively engineered structural disorder, thereby increasing the exposure of active edge sites and improving intrinsic electrical conductivity[36].

Carbon-based materials doped with heteroatoms have also shown remarkable electrocatalytic activity. Dai *et al.* developed nitrogen- and phosphorus-doped carbon networks for oxygen reduction and hydrogen evolution reactions and demonstrated that N- and P-doped graphene exhibited superior HER performance compared with pristine graphene[37]. The enhanced catalytic activity of heteroatom-doped carbon materials is mainly attributed to the electronegativity difference between carbon and the dopant atoms, which induces charge redistribution and generates additional active sites by disturbing the electroneutrality of the carbon framework.

In the present work, defect-rich oxygen-incorporated MoS_2 coupled with nitrogen and phosphorus co-doped reduced graphene oxide (O-MoS_2/N, P-rGO) was successfully synthesised. Oxygen-incorporated MoS_2 was prepared through a facile hydrothermal route, whereas heteroatom-doped reduced graphene oxide was synthesised by physically mixing graphene oxide with nitrogen and phosphorus precursors followed by thermal treatment under an inert atmosphere. The novelty of this study lies in the rational combination of oxygen-defect engineering and dual heteroatom doping within a single hybrid architecture to synergistically enhance the electrocatalytic properties of the composite. The as-prepared O-MoS_2/N, P-rGO composite exhibited superior HER electrocatalytic performance compared with bare O-MoS_2, O-MoS_2/N-rGO, and O-MoS_2/P-rGO, demonstrating the synergistic effect of oxygen defects and dual heteroatom doping toward enhanced hydrogen evolution activity.

2. Experimental Section

Graphene oxide was prepared by the modified Hummers method, which was then utilized for the preparation of heteroatom-doped reduced graphene oxide. In the typical synthesis procedure of Nitrogen, Phosphorus doped

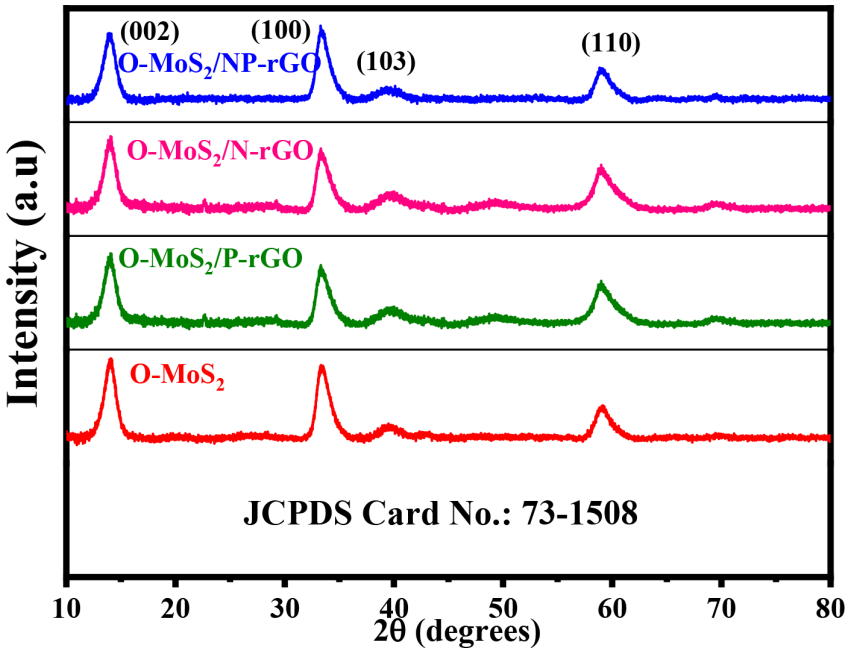


Figure 1. XRD pattern of as-synthesized O-MoS_2, O-MoS_2/P-rGO, O-MoS_2/N-rGO and O-MoS_2/N, P-rGO electrocatalyst corresponding to JCPDS No: 73-1508.

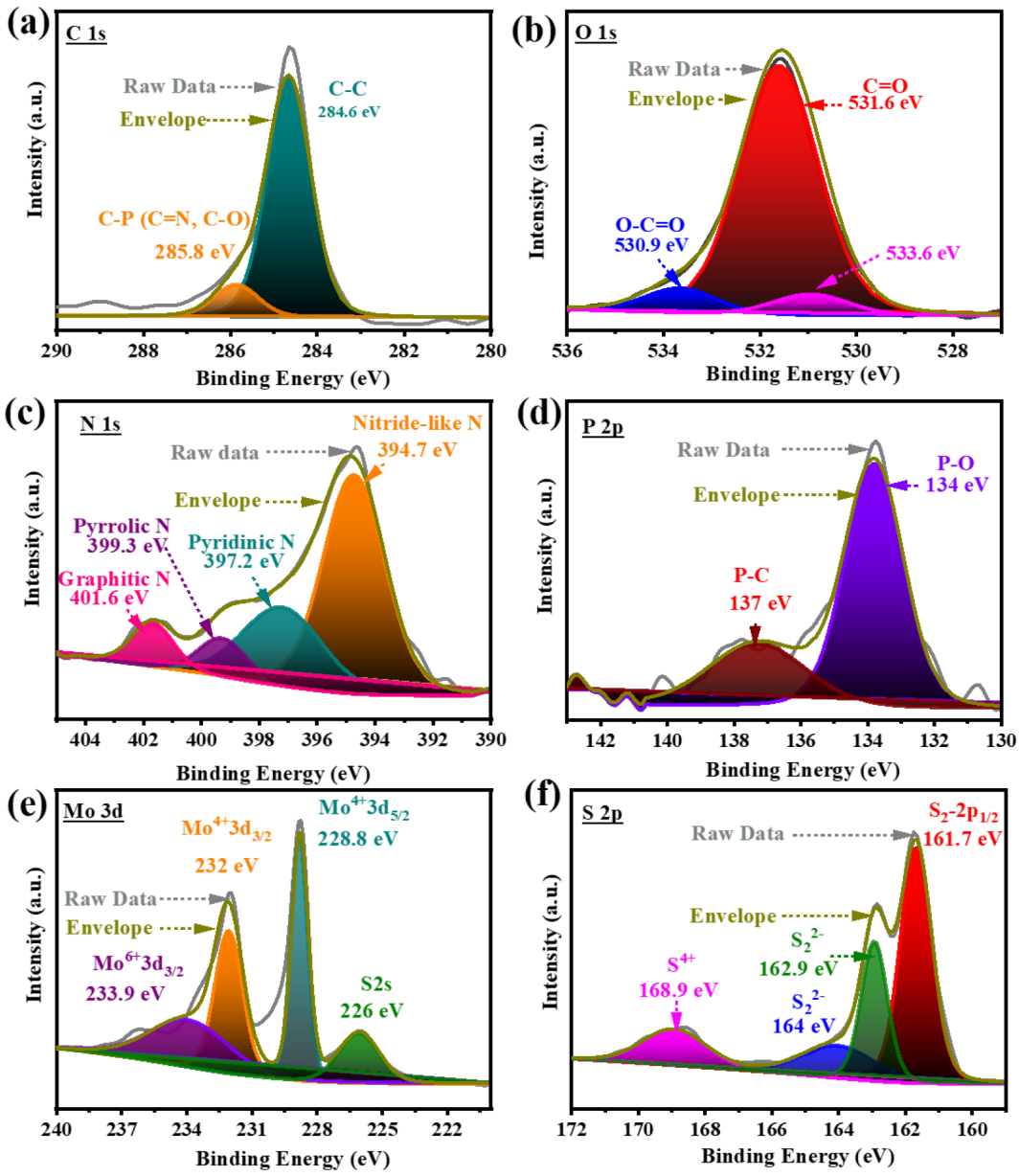


Figure 2. XPS spectra of **(a)** C 1s, **(b)** O 1s, **(c)** N 1s, **(d)** P 2p, **(e)** Mo 3d, and **(f)** S 2p, revealing the core level peak regions.

reduced graphene oxide (N, P-rGO), Melamine and Triphenyl Phosphine were physically mixed with graphene oxide in the ratio of 10:10:1 and subsequently heated at 950°C under Ar atmosphere with a heating ramp of 3°C[38]. Nitrogen-doped reduced graphene oxide (N-rGO) and phosphorus-doped reduced graphene oxide (P-rGO) were prepared under similar conditions without the addition of triphenylphosphine and melamine, respectively.

Oxygen-incorporated MoS_2 was prepared as per the previously reported procedure with slight modification[36]. In detail, 2 mmol of Sodium Molybdate and 60 mmol of Thiourea were dissolved in 70 ml of de-ionised water under vigorous stirring. After continuous stirring for 30 mins, the homogeneous solution was transferred into a 100 ml Teflon lined autoclave and maintained at 180°C for 24 h with no intentional ramping rate. 50 mg of prepared N, P-rGO, N-rGO and P-rGO were added in the synthetic procedure of O-MoS_2 to prepare a composite of O-MoS_2/N, P-rGO, O-MoS_2/N, rGO and O-MoS_2/P, rGO.

3. Material Characterization

The crystal structures of the synthesized samples were analyzed by X-ray diffraction (XRD). Surface

morphology and structural features were examined using Transmission Electron Microscopy (TEM). Surface chemical states and electronic structures were investigated using X-ray Photoelectron Spectroscopy (XPS).

4. Electrochemical Measurement

Electrochemical activity was carried out using a BioLogic SP-300 and a PINE Rotating Disk Electrode (RDE) instrument. N_2 saturated 0.5 M H_2SO_4 (pH=0.33) was used as an electrolyte, whereas RDE Glassy Carbon, Ag/AgCl and Graphite were used as the Working electrode, Reference electrode and Counter Electrode, respectively.

The potential of Ag/AgCl was referenced to RHE using the equation:

$$E_{RHE} = E_{Ag/AgCl} + 0.197+0.059 \times 0.33 - \quad \text{Equation (1)}$$

Electrochemical characterisation was performed using Cyclic Voltammetry and Linear Sweep Voltammetry (LSV). Prior to LSV measurements, the catalyst was electrochemically activated by repeated CV cycles. iR correction was carried out using the Potentiostatic Electrochemical Impedance Spectroscopy

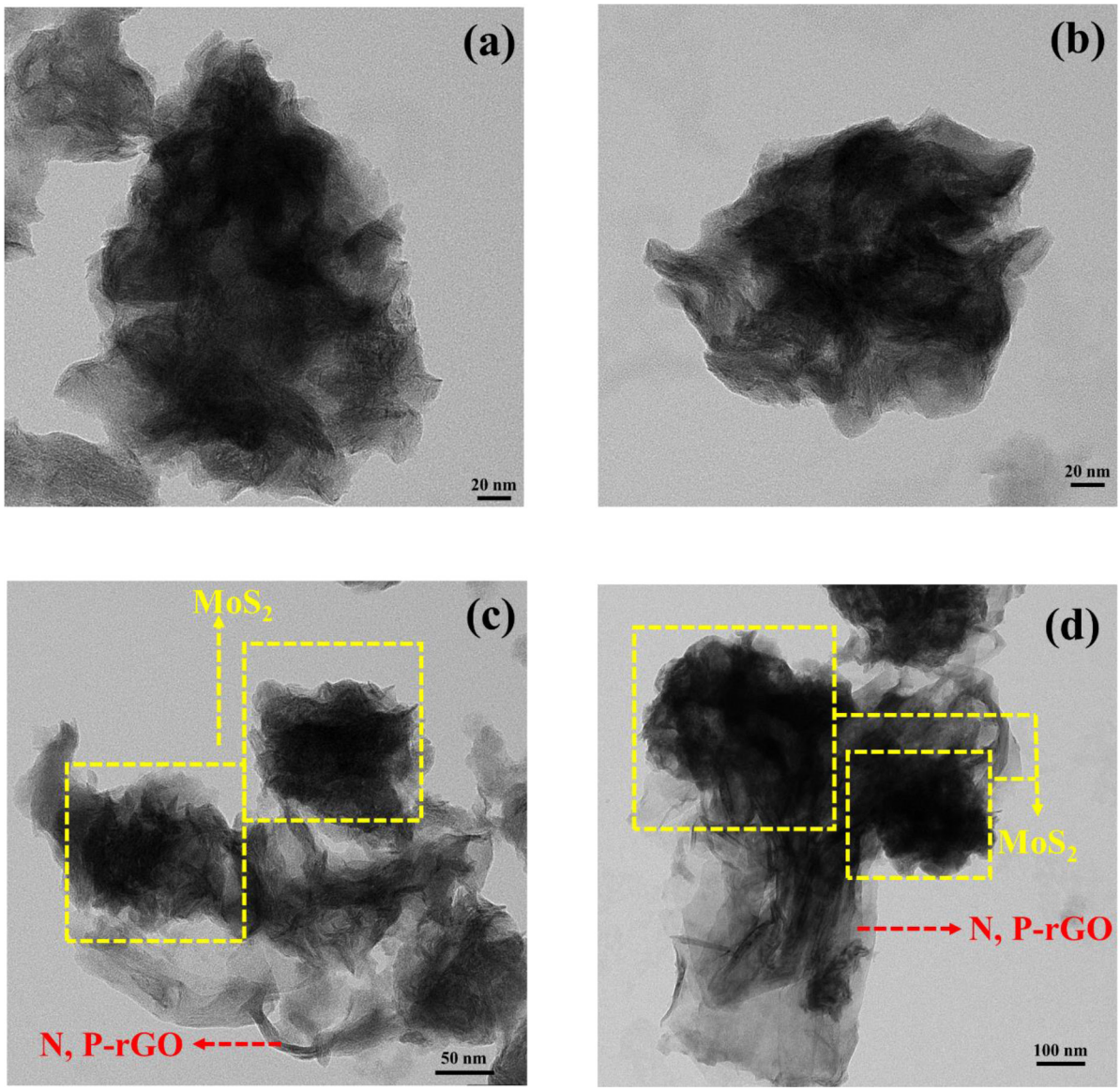


Figure 3. TEM images of (**a** and **b**) O-MoS_2, (**c** and **d**) O-MoS_2/N, P-rGO.

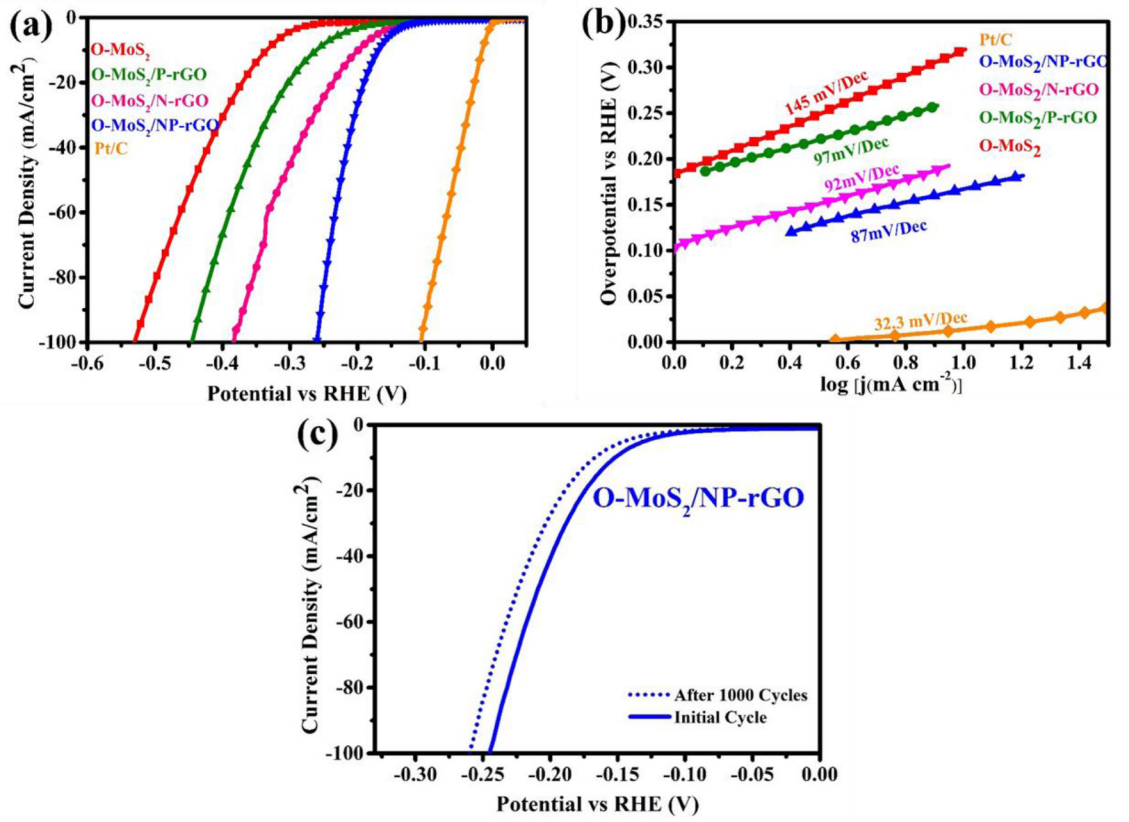


Figure 4. **(a)** Linear Sweep Voltammetry curves (iR corrected) of the electrocatalyst prepared, **(b)** Tafel plots, **(c)** Stability evaluation showing LSV curves before and after 1000 continuous CV cycles.

Table 1. Electrocatalytic HER performance of the catalyst prepared

Catalyst	Onset Potential (mV)	Overpotential @ 10 mA/cm$_2$ (mV)	Tafel Slope (mV/dec)
O-MoS$_2$/N, P-rGO	110	160	87
O-MoS$_2$/N-rGO	160	200	92
O-MoS$_2$/P-rGO	280	260	97
O-MoS$_2$	300	330	145
Pt/C	20	35	38

(PEIS) technique, which is an inbuilt tool in BioLogic SP-300. The fixed frequency of 60 kHz was set in the PEIS technique with 85% of iR compensation for all the catalysts. Henceforth, all the LSV curves shown in Figure 4(a) are 85% iR compensated. Tafel slope values for all the catalysts were calculated from the iR corrected LSV, whereas the stability test was carried out through continuous 1000 cycles.

Table 2. HER performance comparison of MoS_2/carbon electrocatalysts in acidic medium

Catalyst	Over potential @ 10 mA/cm$_2$ (mV)	Tafel Slope (mV/dec)	References
Defect-rich MoS$_2$	10 mA/cm2 (mV)	50	[13]
MoS$_2$/Graphene/Ni-foam	-109	42	[14]
Nanosized bulk MoS$_2$	-280	82	[36]
Pristine MoS$_2$ nanosheets	-210	95	[46]
1T@2H MoS$_2$	-180	88	[47]
Pure MoS$_2$ nanoparticles	-160	77	[48]
MoS$_2$ QDs	-160	58	[49]
Defect-free MoS$_2$	-180	87	[50]
MoS$_2$/Reduced graphene oxide	-100	41	[51]
MoS$_2$/Carbon nanofiber foam	-120	44	[52]

5. Results and Discussion

5.1 Physical Characterisation

X-ray diffraction studies were performed to identify the phase. Figure 1 shows the corresponding XRD patterns that are well matched with the Joint Committee on Powder Diffraction Standards (JCPDS No: 73-1508), which belongs to the 2H Phase and Space Group of P63/mmc (194). No peaks corresponding to rGO were observed, which can be due to the low weight percentage in the nanocomposite.

XPS was further utilized to analyze the chemical state of as-prepared O-MoS_2/N, P-rGO. The spectrum of O-MoS_2/N, P-rGO is clearly represented in Figure 2. The C1s spectra from Figure 2a reveal the presence of Nitrogen as well as phosphorus with the appearance of a peak at 285.8 eV, which indicates the bond formation of C-P (C=N, C-O), whereas an intense peak appeared at 284.6eV reveals the formation of the C-C bond[39-40]. O1s spectra represented in Figure 2b were analysed to differentiate the Oxygen bonded to carbon in rGO and oxygen incorporated in MoS_2. It was clearly indicated that the major peak appearing at 531.6eV was due to the formation of the C=O bond, whereas the peak appearing at 530.9eV was due to the formation of O-C=O. A peak at 533.6eV appeared in addition, which can be mainly due to the incorporated oxygen in MoS_2[41-42]. The oxygen incorporation in MoS_2 was calculated to be 8.0%. N1s spectra exhibited four types of nitrogen species, which are represented in Figure 2c. Four peaks at 394.7 eV, 397.2 eV, 399.3 eV and 401.6 eV reveal the presence of Nitride-like N, Pyridinic N, Pyrrolic N and Graphitic N, respectively[43]. P-C bond formation at 137eV and P-O bond formation at 134eV further confirm the phosphorus doping, which is clearly shown in P2p spectra from Figure 2d[44]. The Mo 3d and S 2s core level peak regions are shown in Figures 2e and f. The Mo 3d spectra show four peaks at 228.8 eV, 232 eV, 233.9 eV and 226 eV. The two peaks at 228.8 eV and 232 eV can be correlated to the doublet Mo $3d_{5/2}$ and Mo $3d_{3/2,}$ whereas the peaks at 233.9eV and 226eV can be correlated to the Mo^{6+} state and S2s state, respectively. The S2p spectra show two major peaks at 162.9eV and 161.7eV corresponding to the S_2^{2-} and S_2-$2p_{1/2}$ states, respectively. The other two peaks located at 168.9eV and 164eV related to S^{4+} and $S_2^{2-,}$ respectively, are the oxidised form of sulphur[45].

TEM images of the synthesised materials are presented in Figures 3(a) to 3(d), and Figures 3(a)-(b) shows the characteristic ultrathin, wrinkled, and sheet-like morphology of MoS_2, indicating the formation of layered nanosheets with slight folding and overlapping. In the MoS_2/N, P-rGO composite (Figures 3(c) and (d)), the MoS_2 nanosheets are well distributed and attached to the transparent, crumpled N, P-rGO sheets, forming an interconnected layered architecture. The N, P-rGO sheets promote the homogeneous dispersion of MoS_2 and effectively suppress the aggregation and restacking of the nanosheets. The intimate interfacial contact between MoS_2 and N, P-rGO is expected to facilitate efficient electron transport while enhancing the structural stability of the composite. TEM observations confirm the successful fabrication of the MoS_2/N, P-rGO heterostructure with a well-integrated layered morphology, which is beneficial for improved electrochemical and electrocatalytic performance.

5.2 Electrochemical Performance

The electrochemical performance of all the catalysts prepared is represented in Figure 4. It is observed that O-MoS_2/N, P-rGO has shown significantly better performance when compared to other heteroatom-doped rGO and O-MoS_2 nanocomposites. From the LSV curve in Figure 4a, it can be concluded that O-MoS_2/N, P-rGO has outperformed the other O-MoS_2-based nanocomposite and bare O-MoS_2 catalyst. The onset potential, overpotential and Tafel slope values of O-MoS_2 have been greatly reduced with the incorporation of N, P-rGO. The onset potential of 110 mV exhibited by O-MoS_2/N, P-rGO outperformed O-MoS_2/N-rGO with 160 mV, O-MoS_2/P-rGO with 280 mV and O-MoS_2 with 300 mV. Whereas the overpotential at 10 mA/cm^2 followed in order as follows: O-MoS_2/N, P-rGO (165mV) < O-MoS_2/N-rGO (200mV) < O-MoS_2/P-rGO (260mV) < O-MoS_2 (3mV).

The mechanism of the catalyst in acidic medium is stated as follows:

Volmer-Heyrovsky: $H_3O^+ + e^- \leftrightarrow Hads + H_2O_{(l)}$ Equation (2)

$H_{ads} + H_3O^+ (l) + e^- \leftrightarrow H_2 (g) + H_2O_{(l)}$

Volmer-Tafel: $H_3O^+_{(l)} + e^- \leftrightarrow H_{ads} + H_2O_{(l)}$ Equation (3)

$H_{ads} + H_{ads} \leftrightarrow H_{2(g)}$

Production of H_2 may occur via two different pathways after adsorption of hydrogen atoms on the surface of the catalyst. One pathway that involves the

direct combination of two H_{ads} is termed the Volmer-Tafel mechanism (combination reaction, Tafel slope ≈ 29 $mVdec^{-1}$). Another part is related to the adsorbed hydrogen atom (H_{ads}), which accepts an electron and then combines with another proton source known as the Volmer-Heyrovsky mechanism (ion + atom reaction, Tafel slope ≈ 38 $mV.dec^{-1}$). H_2 production involving two different pathways after the adsorption of hydrogen atoms on the catalyst can be determined by the Tafel slope value derived from the LSV curve. Figure 4b represents the Tafel slope values of all the catalysts prepared. From the obtained values, it is obvious that O-MoS_2/N, P-rGO, O-MoS_2/N-rGO, O-MoS_2/P-rGO and O-MoS_2 proceed reactions via the Volmer-Heyrovsky mechanism. The Tafel slope values calculated in order are as follows: O-MoS_2/N, P-rGO (87 $mVdec^{-1}$) < O-MoS_2/N-rGO (92 $mVdec^{-1}$) < O-MoS_2/P-rGO (97 $mVdec^{-1}$) < O-MoS_2 (145 $mVdec^{-1}$). From the obtained values, it is clear that the rate kinetics of O-MoS_2 has become much faster with the incorporation of N, P-rGO. Even though Pt/C (20 wt.%) has exhibited the faster reaction kinetics with Volmer-Tafel mechanism, the effort towards the increasing rate kinetics of MoS_2 has been successfully implemented with the incorporation of Oxygen and making a nanocomposite with N, P-rGO. Table 1 lists the overall electrocatalytic performance of the catalysts prepared. The stability test, as shown in Figure 4c, was carried out through continuous CV cycling. O-MoS_2/N, P-rGO was continuously subjected to a potential range from 0.1V to -0.5V vs Ag/AgCl. The stability was tested up to the current density of 100 mA/cm^2. It is worth noting that the small shift in potential was observed even after 1000 continuous cycles, which revealed near-stable performance of O-MoS_2/N, P-rGO.

The HER performance of various MoS_2-based electrocatalysts reported in the literature is summarised in Table 2. Pristine MoS_2 nanosheets exhibit an overpotential of 210 mV at 10 mA m^{-2} with a Tafel slope of 95 mV dec_{-1}, indicating relatively sluggish hydrogen evolution kinetics. Significant improvements are observed through phase engineering, defect creation, and hybridisation with conductive carbon materials. The 1T@2H MoS_2 heterophase catalyst shows a reduced overpotential of 180 mV and a Tafel slope of 88 mV dec_{-1} due to enhanced electrical conductivity. Defect-rich MoS_2 demonstrates superior catalytic activity compared to defect-free MoS_2, requiring only 120 mV overpotential and exhibiting a lower Tafel slope of 50mV dec^{-1}, highlighting the critical role of sulfur vacancies and defect sites in providing additional active centres for hydrogen adsorption. Furthermore, incorporating conductive carbon supports such as reduced graphene oxide, carbon nanofiber foam, and graphene/Ni foam substantially enhances electron transport and catalyst utilization. Among the reported catalysts, MoS_2/rGO exhibits the best HER performance with a low overpotential of 100 mV and a Tafel slope of 41 mV dec_{-1}, followed closely by MoS_2/graphene/Ni foam (109 mV, 42 mV dec_{-1}). These results clearly demonstrate that defect engineering and the construction of conductive heterostructures effectively optimize the intrinsic activity and charge-transfer characteristics of MoS_2, leading to accelerated HER kinetics and improved electrocatalytic performance.

6. Conclusion

The overall HER performance of O-MoS_2/N, P-rGO was systematically evaluated through LSV, durability testing, and Tafel analysis. The catalyst exhibited a significantly enhanced electrocatalytic activity, delivering a low onset potential of 110 mV, an overpotential of only 160 mV at 10 mA cm^{-2}, and a Tafel slope of 87 mV dec^{-1}, indicating favourable hydrogen evolution kinetics. The improved performance confirms that the strategy of oxygen incorporation and N, P-rGO integration effectively mitigates the inherently poor conductivity of the semiconducting 2H-MoS_2 phase. Furthermore, the catalyst demonstrated excellent electrochemical stability during repeated LSV cycling, highlighting its robust structural integrity under HER operating conditions. XPS provided direct evidence for successful oxygen incorporation into the MoS_2 framework. In particular, the appearance of an additional O 1s peak at 533.6eV was attributed to oxygen species incorporated within the MoS_2 lattice, clearly distinguishing it from oxygen-containing functional groups associated with the N, P-rGO support. The synergistic effect of oxygen incorporation and the conductive N, P-rGO network enhances charge transfer, increases the density of active sites, and ultimately leads to superior HER performance.

7. References

1. Lukowski MA, Daniel AS, Meng F, Forticaux A, Li L, Jin S. Enhanced hydrogen evolution catalysis from chemically exfoliated metallic MoS2 nanosheets. J Am Chem Soc. 2013; 135(28):10274-10277. https://doi.org/10.1021/ja404523s PMID:23790049.

2. Zhu H, Lyu F, Du M, Zhang M, Wang Q, Yao J, Guo B. Design of two-dimensional, ultrathin MoS2 nanoplates fabricated within one-dimensional carbon nanofibers with thermosensitive morphology: High-performance electrocatalysts for the hydrogen evolution reaction. ACS Appl Mater Interfaces. 2014; 6(24):22126-22137. https://doi.org/10.1021/am505544g PMID:25420219.
3. Zhang X, Li L, Guo Y, Liu D, You T. Amorphous flower-like molybdenum-sulfide-@-nitrogen-doped-carbon-nanofiber film for use in the hydrogen-evolution reaction. J Colloid Interface Sci. 2016; 472:69-75. https://doi.org/10.1016/j.jcis.2016.03.041 PMID:27015391.
4. Yazici B. Hydrogen evolution at platinum (Pt) and at platinized platinum (Ptz) cathodes. Turk J Chem. 1999; 23(3):301-308.
5. Tavares MC, Machado SA, Mazo LH. Study of hydrogen evolution reaction in acid medium on Pt microelectrodes. Electrochim Acta. 2001; 46(28):4359-4369. https://doi.org/10.1016/S0013-4686(01)00726-5
6. Jaksica J, Vracara L, Neophytidesb SG, Krstajica N. Electrocatalytic behaviour of MoPt3 intermetallic phase for hydrogen evolution in acid solution. J New Mater Electrochem Syst. 2004; 7(3):205-212.
7. Ortega-Chavez L, Herrera-Peraza E, Verde Y. Hydrogen evolution reaction on electrodes with different Pt/C loadings by electrochemical impedance spectroscopy. J New Mater Electrochem Syst. 2008; 11.
8. Aruna KK, Manoharan R. Electrochemical hydrogen evolution catalyzed by SrMoO4 spindle particles in acid water. Int J Hydrogen Energy. 2013; 38(29):12695-12703. https://doi.org/10.1016/j.ijhydene.2013.07.064
9. Vrubel H, Hu X. Molybdenum boride and carbide catalyze hydrogen evolution in both acidic and basic solutions. Angew Chem Int Ed. 2012; 51:12703-12706. https://doi.org/10.1002/anie.201207111 PMID:23143996.
10. Jaramillo TF, Bonde J, Zhang J, Ooi BL, Andersson K, Ulstrup J, Chorkendorff I. Hydrogen evolution on supported incomplete cubane-type [Mo3S4]4+ electrocatalysts. J Phys Chem C. 2008; 112(45):17492-17498. https://doi.org/10.1021/jp802695e
11. Shen X, Pantelides ST. Atomic-scale mechanism of efficient hydrogen evolution at SiC nanocrystal electrodes. J Phys Chem Lett. 2013;4(1):100-104. https://doi.org/10.1021/jz301799w PMID:26291219.
12. McKone JR, Sadtler BF, Werlang CA, Lewis NS, Gray HB. Ni-Mo nanopowders for efficient electrochemical hydrogen evolution. ACS Catal. 2013; 3(2):166-169. https://doi.org/10.1021/cs300691m
13. Li Y, Wang H, Xie L, Liang Y, Hong G, Dai H. MoS2 nanoparticles grown on graphene: An advanced catalyst for the hydrogen evolution reaction. J Am Chem Soc. 2011; 133(19):7296-7299. https://doi.org/10.1021/ja201269b PMID:21510646.
14. Xie J, Zhang J, Li S, Grote F, Zhang X, Zhang H, Wang R, Lei Y, Pan B, Xie Y. Controllable disorder engineering in oxygen-incorporated MoS2 ultrathin nanosheets for efficient hydrogen evolution. J Am Chem Soc. 2013; 135(47):17881-17888. https://doi.org/10.1021/ja408329q PMID:24191645.
15. Dai X, Du K, Li Z, Sun H, Yang Y, Zhang X, Li X, Wang H. Highly efficient hydrogen evolution catalysis by MoS2-MoN/carbonitride composites derived from tetrathiomolybdate/polymer hybrids. Chem Eng Sci. 2015; 134:572-580. https://doi.org/10.1016/j.ces.2015.05.065.
16. Lai F, Miao YE, Huang Y, Zhang Y, Liu T. Nitrogen-doped carbon nanofiber/molybdenum disulfide nanocomposites derived from bacterial cellulose for high-efficiency electrocatalytic hydrogen evolution reaction. ACS Appl Mater Interfaces. 2016;8(6):3558-3566. https://doi.org/10.1021/acsami.5b06274 PMID:26302501.
17. Yan Y, Xia B, Ge X, Liu Z, Wang JY, Wang X. Ultrathin MoS2 nanoplates with rich active sites as highly efficient catalyst for hydrogen evolution. ACS Appl Mater Interfaces. 2013;5(24):12794-12798. https://doi.org/10.1021/am404843b PMID:24299040.
18. Yan Y, Xia B, Li N, Xu Z, Fisher A, Wang X. Vertically oriented MoS2 and WS2 nanosheets directly grown on carbon cloth as efficient and stable 3-dimensional hydrogen-evolving cathodes. J Mater Chem A. 2015; 3(1):131-135. https://doi.org/10.1039/C4TA04858J.
19. Yang L, Zhou W, Hou D, Zhou K, Li G, Tang Z, Li L, Chen S. Porous metallic MoO2-supported MoS2 nanosheets for enhanced electrocatalytic activity in the hydrogen evolution reaction. Nanoscale. 2015; 7(12):5203-5208. https://doi.org/10.1039/C4NR06754A PMID:25700339.
20. Zhou W, Hou D, Sang Y, Yao S, Zhou J, Li G, Liu H, Chen S. MoO2 nanobelts@ nitrogen self-doped MoS2 nanosheets as effective electrocatalysts for hydrogen evolution reaction. J Mater Chem A. 2014; 2(29):11358-11364. https://doi.org/10.1039/C4TA01898B
21. Yan Y, Zhang L, Qi X, Song H, Wang JY, Zhang H, Wang X. Template-free pseudomorphic synthesis of tungsten carbide nanorods. Small. 2012; 8(21):3350-3356. https://doi.org/10.1002/smll.201200877 PMID:22829441.
22. Wan C, Regmi YN, Leonard BM. Multiple phases of molybdenum carbide as electrocatalysts for the hydrogen evolution reaction. Angew Chem. 2014; 126(25):6525-6528. https://doi.org/10.1002/ange.201402998
23. Xiao P, Sk MA, Thia L, Ge X, Lim RJ, Wang JY, Lim KH, Wang X. Molybdenum phosphide as an efficient electrocatalyst for the hydrogen evolution reaction. Energy Environ Sci. 2014;7(8):2624-2629. https://doi.org/10.1039/C4EE00957F

24. Kibsgaard J, Jaramillo TF. Molybdenum phosphosulfide: An active, acid-stable, earth-abundant catalyst for the hydrogen evolution reaction. Angew Chem Int Ed. 2014;53(52):14433-14437. https://doi.org/10.1002/anie.201408222 PMID:25359678.
25. Cao B, Veith GM, Neuefeind JC, Adzic RR, Khalifah PG. Mixed close-packed cobalt molybdenum nitrides as non-noble metal electrocatalysts for the hydrogen evolution reaction. J Am Chem Soc. 2013; 135(51):19186-19192 https://doi.org/10.1021/ja4081056 PMID:24175858.
26. Chen WF, Sasaki K, Ma C, Frenkel AI, Marinkovic N, Muckerman JT, Zhu Y, Adzic RR. Hydrogen-evolution catalysts based on non-noble metal nickel-molybdenum nitride nanosheets. Angew Chem Int Ed. 2012; 51(25):6131-6135. https://doi.org/10.1002/anie.201200699 PMID:22565496.
27. Jothi VR, Bose R, Rajan H, Jung C, Yi SC. Harvesting electronic waste for the development of highly efficient eco-design electrodes for electrocatalytic water splitting. Adv Energy Mater. 2018;8(34):1802615. https://doi.org/10.1002/aenm.201802615
28. Bose R, Jothi VR, Koh B, Jung C, Yi SC. Molybdenum sulphoselenophosphide spheroids as an effective catalyst for hydrogen evolution reaction. Small. 2018; 14(8):1703862. https://doi.org/10.1002/smll.201703862 PMID:29318738.
29. Hinnemann B, Moses PG, Bonde J, Jørgensen KP, Nielsen JH, Horch S, Chorkendorff I, Nørskov JK. Biomimetic hydrogen evolution: MoS2 nanoparticles as catalyst for hydrogen evolution. J Am Chem Soc. 2005; 127(15):5308-5309. https://doi.org/10.1021/ja0504690 PMID:15826154.
30. Tsai C, Abild-Pedersen F, Nørskov JK. Tuning the MoS2 edge-site activity for hydrogen evolution via support interactions. Nano Lett. 2014; 14(3):1381-1387. https://doi.org/10.1021/nl404444k PMID:24499163.
31. Zheng Y, Jiao Y, Jaroniec M, Qiao SZ. Advancing the electrochemistry of the hydrogen-evolution reaction through combining experiment and theory. Angew Chem Int Ed. 2015; 54(1):52-65. https://doi.org/10.1002/anie.201407031 PMID:25384712.
32. Bonde J, Moses PG, Jaramillo TF, Nørskov JK, Chorkendorff I. Hydrogen evolution on nano-particulate transition metal sulfides. Faraday Discuss. 2009; 140:219-231. https://doi.org/10.1039/B803857K PMID:19213319.
33. Guo X, Hou Y, Ren R, Chen J. Temperature-dependent crystallization of MoS2 nanoflakes on graphene nanosheets for electrocatalysis. Nanoscale Res Lett. 2017; 12(1):479. https://doi.org/10.1186/s11671-017-2248-9 PMID:28789483.
34. Zhou J, Fang G, Pan A, Liang S. Oxygen-incorporated MoS2 nanosheets with expanded interlayers for hydrogen evolution reaction and pseudocapacitor applications. ACS Appl Mater Interfaces. 2016; 8(49):33681-33689. https://doi.org/10.1021/acsami.6b11811 PMID:27960365.
35. Morales-Guio CG, Hu X. Amorphous molybdenum sulfides as hydrogen evolution catalysts. Acc Chem Res. 2014; 47(8):2671-2681. https://doi.org/10.1021/ar5002022 PMID:25065612.
36. Xie J, Zhang H, Li S, Wang R, Sun X, Zhou M, Zhou J, Lou XW, Xie Y. Defect-rich MoS2 ultrathin nanosheets with additional active edge sites for enhanced electrocatalytic hydrogen evolution. Adv Mater. 2013; 25(40):5807-5813. https://doi.org/10.1002/adma.201302685 PMID:23943511.
37. Zhang N, Gan S, Wu T, Ma W, Han D, Niu L. Growth control of MoS2 nanosheets on carbon cloth for maximum active edges exposed: An excellent hydrogen evolution 3D cathode. ACS Appl Mater Interfaces. 2015; 7(22):12193-12202. https://doi.org/10.1021/acsami.5b02586 PMID:25980786.
38. Zou X, Zhang Y. Noble metal-free hydrogen evolution catalysts for water splitting. Chem Soc Rev. 2015; 44(15):5148-5180. https://doi.org/10.1039/C4CS00448E. PMID:25886650.
39. Li K, Chen S, Chen S, Liu X, Pan W, Zhang J. Nitrogen, phosphorus co-doped carbon cloth as self-standing electrode for lithium-iodine batteries. Nano Res. 2019; 12(3):549-555. https://doi.org/10.1007/s12274-018-2251-1.
40. Xia B, Yan Y, Wang X, Lou XW. Recent progress on graphene-based hybrid electrocatalysts. Mater Horiz. 2014; 1(4):379-399. https://doi.org/10.1039/C4MH00040D
41. Zheng X, Xu J, Yan K, Wang H, Wang Z, Yang S. Space-confined growth of MoS2 nanosheets within graphite: The layered hybrid of MoS2 and graphene as an active catalyst for hydrogen evolution reaction. Chem Mater. 2014; 26(7):2344-2353. https://doi.org/10.1021/cm500347r
42. Zhou W, Zhou K, Hou D, Liu X, Li G, Sang Y, Liu H, Li L, Chen S. Three-dimensional hierarchical frameworks based on MoS2 nanosheets self-assembled on graphene oxide for efficient electrocatalytic hydrogen evolution. ACS Appl Mater Interfaces. 2014;6(23):21534-21540. https://doi.org/10.1021/am506545g PMID:25347618.
43. Gong F, Ye S, Liu M, Zhang J, Gong L, Zeng G, Meng E, Su P, Xie K, Zhang Y, Liu J. Boosting electrochemical oxygen evolution over yolk-shell structured O-MoS2 nanoreactors with sulfur vacancy and decorated Pt nanoparticles. Nano Energy. 2020; 78:105284. https://doi.org/10.1016/j.nanoen.2020.105284
44. Zhang J, Qu L, Shi G, Liu J, Chen J, Dai L. N,P-codoped carbon networks as efficient metal-free bifunctional catalysts for oxygen reduction and hydrogen evolution reactions. Angew Chem Int Ed. 2016; 55(6):2230-2234. https://doi.org/10.1002/anie.201510495 PMID:26709954.
45. Hao X, Jiang Z, Tian X, Hao X, Maiyalagan T, Jiang ZJ. A novel particle-in-nanoplate architecture of iron nickel phosphide intertwined with carbon nanotubes for efficient

water oxidation and high-performance sodium-ion batteries. J Alloys Compd. 2019; 791:1220-1230. https://doi.org/10.1016/j.jallcom.2019.03.311

46. Tang C, Wang W, Sun A, Qi C, Zhang D, Wu Z, Wang D. Sulfur-decorated molybdenum carbide catalysts for enhanced hydrogen evolution. ACS Catal. 2015; 5(11):6956-6963. https://doi.org/10.1021/acscatal.5b01803
47. Liu J, Zheng Y, Zhu D, Vasileff A, Ling T, Qiao SZ. Identification of pH-dependent synergy on Ru/MoS2 interface: A comparison of alkaline and acidic hydrogen evolution. Nanoscale. 2017; 9(43):16616-16621. https://doi.org/10.1039/C7NR06111K PMID:29075731.
48. Yao Y, Ao K, Lv P, Wei Q. MoS2 coexisting in 1T and 2H phases synthesized by common hydrothermal method for hydrogen evolution reaction. Nanomaterials. 2019; 9(6):844. https://doi.org/10.3390/nano9060844 PMID:31159477.
49. Wang T, Gao D, Zhuo J, Zhu Z, Papakonstantinou P, Li Y, Li M. Size-dependent enhancement of electrocatalytic oxygen-reduction and hydrogen-evolution performance of MoS2 particles. Chem Eur J. 2013; 19(36):11939-11948. https://doi.org/10.1002/chem.201301406 PMID:23873743.
50. Ren X, Pang L, Zhang Y, Ren X, Fan H, Liu SF. One-step hydrothermal synthesis of monolayer MoS2 quantum dots for highly efficient electrocatalytic hydrogen evolution. J Mater Chem A. 2015; 3(20):10693-10697. https://doi.org/10.1039/C5TA02198G
51. Chang YH, Lin CT, Chen TY, Hsu CL, Lee YH, Zhang W, Wei KH, Li LJ. Highly efficient electrocatalytic hydrogen production by MoSx grown on graphene-protected 3D Ni foams. Adv Mater. 2013; 25(5):756-760. https://doi.org/10.1002/adma.201202920 PMID:23060076.
52. Guo X, Cao GL, Ding F, Li X, Zhen S, Xue YF, Yan YM, Liu T, Sun KN. A bulky and flexible electrocatalyst for efficient hydrogen evolution based on the growth of MoS2 nanoparticles on carbon nanofiber foam. J Mater Chem A. 2015; 3(9):5041-5046. https://doi.org/10.1039/C5TA00087D

Author Contribution

K.G.: Conceptualization, Methodology, Formal analysis, Writing–original draft, Visualization; **T.M.:** Supervision, writing–review and editing, Validation.